Focusing X-rays with simple arrays of prism-like structures

Werner Jark,[a]* Fréderic Pérennès,[a] Marco Matteucci,[b] Lucia Mancini,[a] Francesco Montanari,[c] Luigi Rigon,[d] Giuliana Tromba,[a] Andrea Somogyi,[e] Remi Tucoulou[e] and Sylvain Bohic[e]

[a]Sincrotrone Trieste ScpA, SS 14 km 163.5, 34012 Basovizza (TS), Italy, [b]INFM-TASC, SS 14 km 163.5, 34012 Basovizza (TS), Italy, [c]ASP, Viale Settimio Severo 65, 10133 Torino (TO), Italy, [d]Dipartimento di Fisica, Università di Trieste e INFN, Via Valerio 2, I-34100 Trieste (TS), Italy, and [e]European Synchrotron Radiation Facility ESRF, BP 220, 38043 Grenoble CEDEX, France. E-mail: werner.jark@elettra.trieste.it

This report discusses the optimization strategy, the theoretical background and first experimental data of a new refractive lens for focusing X-rays. In order to reduce the absorption of X-rays in this transmission lens, optically passive material was removed from the necessarily concave lens shape in a highly regular pattern. The feature dimensions require lens production and replication by deep X-ray lithography, which allows shaping in only one dimension. Consequently such a lens can focus in one direction only, so a crossed lens pair is needed for two-dimensional focusing. The single lens is composed of two large prisms of millimetre size, which touch each other at one of the tips, like an old sand clock. Each large prism contains a highly regular structure of essentially identical prism-like smaller segments. The first lens prototypes focused an X-ray beam with a vertical size of 500 μm and a photon energy of 8 keV to a line with a width of only 2.8 μm. This is only slightly worse than the line width of 1.73 μm expected for its focal length of f = 2.18 m. The photon density enhancement in the focus was 25, but could have been larger as the lens can intercept a beam height of 2.6 mm.

Keywords: X-ray optics; transmission lenses; focusing; deep X-ray lithography; diffraction gratings.

1. Introduction

The principle purpose of focusing optics to be used in combination with X-rays is to provide the highest possible flux in a spot as small as possible. One criterion for the comparison of different optics is thus the observed spot size. In the case of equivalent spot sizes a system is more efficient if it has a larger effective aperture, as introduced by Lengeler, Schroer, Tuemmler *et al.* (1999). This effective aperture is the aperture of a completely transparent optical system, which intercepts the same photon flux, that is found in the focus of an absorbing lens. Obviously the effective aperture is usually smaller and will at best be identical to the geometrical aperture of an optical system. This effective aperture can be calculated for the different optics and it can be obtained from experimental data by multiplying the area of the focal spot by the observed photon flux density enhancement (*i.e.* gain).

State-of-the-art spot sizes in the X-ray range (several keV photon energy) are of the order of 50 nm. This value was provided by beam-compressing capillaries (Bilderback *et al.*, 1994), while more recently beam-compressing X-ray waveguides have provided slightly smaller values in one- (Jark *et al.*, 2001) and two-dimensionally (Pfeiffer *et al.*, 2002) compressing devices. Reflective Kirkpatrick–Baez mirror pairs (Kirkpatrick & Baez, 1948) produced spots of diameter <90 nm (Hignette *et al.*, 2004) and refractive transmission lenses achieved spot sizes of 210 nm in one direction (Schroer *et al.*, 2003). Fresnel zone-plates can provide similar numbers in the X-ray range, and they routinely provide values of the order of 25 nm below 1 keV photon energy (Di Fabrizio *et al.*, 1999; Yun *et al.*, 1999). In all these cases the calculated effective apertures and those derived from the experimental data are <1 mm for one-dimensional focusing, and the corresponding effective collection areas are <0.1 mm^2 for two-dimensional focusing. This is because the optics rarely provide geometric apertures of the order of 1 mm for the beam collection. In addition, the focusing efficiency is often found to be appreciably smaller than 1. This report presents data for a new transmission lens with reduced absorption for one-dimensional focusing, which provides a geometric aperture of several millimetres in the focusing direction.

Transmission lenses are the most appreciated optical system for the focusing of radiation beams throughout the electromagnetic spectrum as they can be inserted readily into optical instruments. As far as X-rays are concerned, Kirkpatrick & Baez (1948) proposed a stack of curved surfaces in the most promising material, beryllium, for the focusing of X-rays. Such a stack of N biconcave lenses with identical radius of curvature R provides a focal length of

$$f = R/(2N\delta). \quad (1)$$

Here, δ is the unit decrement of the refractive index n of the material, which for X-rays is usually written as $n = 1 - \delta + i\beta$. For a mixture, δ is given by (Henke *et al.*, 1993)

$$\delta = \left(r_e\lambda^2/2\pi\right)\sum_i N_i f_{1,i}, \quad (2)$$

where $r_e = 2.818 \times 10^{-15}$ m is the classical electron radius, λ is the wavelength and N_i is the number of atoms of a particular element i per unit volume, while $f_{1,i}$ is the related element-specific atomic scattering factor, which is tabulated (Henke *et al.*, 1993; Chantler *et al.*, 2003). Wavelength λ and photon energy E are related *via* λE = 1239.852 nm eV.

Actually, Kirkpatrick & Baez (1948) abandoned the transmission lenses in favour of the crossed mirror pair as they derived unpractical focal lengths of about f = 100 m for the collection of X-ray tube radiation with λ = 0.071 nm (17.5 keV). The transmission-lens proposal was revived (Suehiro *et al.*, 1991; Yang, 1993) only when undulators at synchrotron radiation laboratories could concentrate X-rays into narrow cones. The simplest and finally technologically feasible X-ray transmission lenses were described by Tomie (1994). They are an array of concave lenses formed by the material left between a series of circular drilled holes of very small diameter. Their first practical realization dates to soon after (Snigirev *et al.*, 1996), when they were named compound refractive lenses (CRL). Clearly the aperture of the original X-ray transmission lens in Fig. 1(*a*) cannot exceed the hole diameter of 0.6 mm and absorption made it much smaller. The absorption losses cannot be reduced much if the ideally focusing lens of parabolic shape (Lengeler, Schroer *et al.*, 1999) (Fig. 1*b*) is used. However, these losses can be minimized in lenses, which are lightened by using the classical strategy of Fresnel of removing passive material, as proposed by Yang (1993) and Lengeler, Schroer, Tuemmler *et al.* (1999). Such lenses were first realized by Aristov *et al.* (2000) using deep X-ray lithographic techniques. Figs. 1(*c*) and 1(*d*) present possible solutions for single lenses, also known as kinoform lenses (Lesem *et al.*, 1969). More recently, stacks of lenses with subsequently shorter focal lengths have been fabricated using the scheme in Fig. 1(*e*) (Snigireva *et al.*, 2001). As these latter

  DOI: 10.1107/S0909049504005825

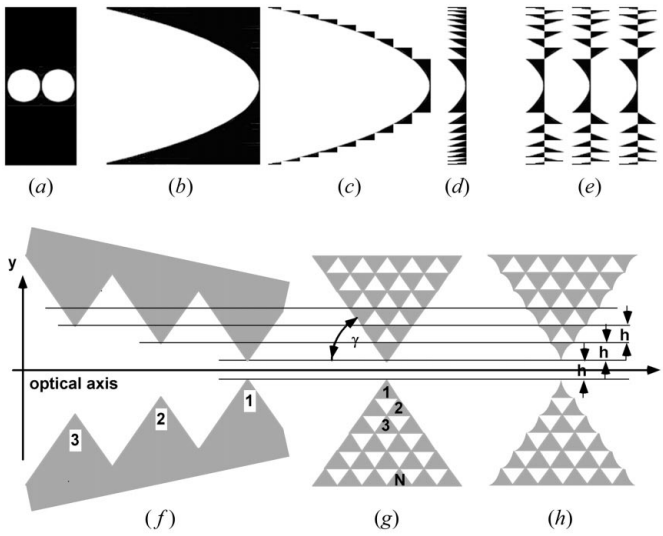

Figure 1
Evolution of transparent concave lenses for the focusing of X-rays. The pioneering experiments were performed using circular holes drilled into a substrate (Snigirev *et al.*, 1996) as shown in (*a*). Single (*b*) or stacks of parabolic lenses provide better focusing properties (Lengeler, Schroer, Tuemmler *et al.*, 1999) and the kinoform version of these objects, (*c*), (*d*) (Aristov *et al.*, 2000) and (*e*) (Snigireva *et al.*, 2001), provide larger apertures owing to reduced absorption. The LP lens (*f*) approximates the parabolic material distribution stepwise (step *h*) with linear segments (Cederström *et al.*, 2000). The focal distance is tunable as *h* can be varied. Note that for the sake of clarity this lens is drawn with a very exaggerated inclination. The prism array (*g*) is the Fresnel version of the latter lens with increased aperture. The array (*h*), which also has the appropriate curvature for ideal focusing, is discussed in this report. The lenses in (*a*) and (*b*) have already been realized with radial symmetry for two-dimensional focusing. All other devices are linear devices, which provide two-dimensional focusing only in a crossed pair.

kinoform lenses focus in only one direction, it will be shown here that their geometric aperture is determined by technological limitations, *i.e.* by the depth into which the outermost and smallest segment can be transferred uniformly into the material. If the removal of passive material can be made such that the size or width of the remaining structures will increase, then the corresponding lens could be realized over a larger depth. This report will discuss in the following the theoretical feasibility of such an approach. Subsequently it will present the practical advantages and the drawbacks of one of the possible lens concepts with a very particular design.

2. Theoretical considerations

Lengeler, Schroer, Tuemmler *et al.* (1999) introduced the effective aperture $A_{\rm eff}$ for two-dimensional focusing. The present discussion will instead deal with single one-dimensionally focusing objects. In this case the theoretical effective aperture is the lens transmission function $t(y)$ integrated over the lens aperture $y_1 < y < y_2$, *i.e.*

$$A_{\rm eff} = \int_{y_1}^{y_2} t(y)\,{\rm d}y. \tag{3}$$

The use of the transmission function is not limited to the case of transparent lenses, but $t(y)$ can also be used to describe the reflectivity of a mirror or the efficiency of a diffracting structure. For a transparent lens with $t(y) = 1$, the effective aperture is identical to the geometrical aperture $A_{\rm eff}\{t(y) = 1\} = y_2 - y_1 = A_{\rm geo}$. In the biconcave version of the parabolic cylinder lens of Fig. 1(*b*) with no material on the optical axis ($d = 0$), one has

$$t(y) = \exp\left(-y^2/2f\delta L\right), \tag{4}$$

where L is the attenuation length in the lens material (Henke *et al.*, 1993). The integration in an oversized aperture out to where $t(y) \simeq 0$ yields the effective aperture

$$A_{\rm eff} = (2\pi f\delta L)^{1/2}. \tag{5}$$

For this type of lens one can also calculate the aperture A', which transmits 90% of the ultimately transmittable photon flux,

$$A' = (3.445\pi f\delta L)^{1/2}. \tag{6}$$

In the case where the lens thickness d in its centre is finite, the lens thickness will be increased uniformly by this amount. Then the optical system is equivalent to the perfect system with $d = 0$ positioned behind a filter of uniform thickness Nd. This will not affect the result for A'; however, the effective aperture $A_{\rm eff}$ has to be multiplied by $\exp(-Nd/L) < 1$.

The present optimization is obtained when passive material is removed from the innovative lens as in Fig. 1(*f*), in which Cederström *et al.* (2000) approximate the parabolic lens shape stepwise with linear segments. As the realization of this exotic lens is as simple as placing two pieces of an old long-playing record (LP) inclined with respect to each other, they are the most economic X-ray lenses. Aperturewise, the lens is a parabolic lens as in Fig. 1(*b*) with $d = 0$.

Passive material for the scope of focusing is any block of material that will change the phase of the traversing wave compared with hypothetical travel in air/vacuum by an integer multiple m of 2π (Yang, 1993). The corresponding material thickness is given by

$$D(y) = m\lambda/\delta. \tag{7}$$

Moving radially away from the centre of a concave lens, passive material can be removed in steps whenever the original amount of material exceeds the quantity given by (7) for increasing m. This was carried out in the reported objects in Figs. 1(*c*)–1(*d*) with constant Δm at the positions given by

$$y_m = (2mf\lambda)^{1/2}. \tag{8}$$

Then the maximum segment thickness in beam direction is constant and given by (7), and the segment height for $m >> 1$ is given by $\Delta y_m = 0.5 y_m \Delta m/m$, which decreases for constant Δm at increasing distance y_m from the lens centre. The averaged amount of remaining material is approximately constant in the lens and is given by $\Delta m\lambda/2\delta$. Consequently the transmission function is approximately identical to that of a filter. Thus the absorption does not limit the aperture in the focusing direction. Instead it will be limited by technological problems. The structures can only be produced by deep X-ray lithography. The aspect ratio P, *i.e.* the ratio between the structure height or depth and its smallest feature width, is limited in this case to about $P = 25$ for isolated structures. As deep X-ray lithography cannot shape in the third dimension, two-dimensional focusing is only provided behind a crossed lens pair. This limits the object aperture A in both directions to the possible feature depth $P\Delta y_m$. It can be shown that this aperture is limited to

$$A = (2Pf\lambda\Delta m)^{1/2}, \tag{9}$$

which is material independent. With $P = 25$ and for rather large $f = 2m$, $\lambda = 0.154$ nm (8 keV) and $\Delta m = 1$, one obtains a small value of about $A = 0.125$ mm. This can be increased at the expense of increased absorption in two ways. First, the same final focal length can be obtained in a stack of N lenses with correspondingly larger individual focal length Nf. Then A increases proportional to $N^{1/2}$.

The alternative solution, in which one allows Δm to increase, is discussed here.

Cederström *et al.* (2000) derived a beam deflection in the single symmetric prisms of the LP lens (Fig. 1*f*) of

$$\Delta = -2\delta/\tan\gamma. \tag{10}$$

Here γ is the angle of grazing incidence onto the prism side walls. Two identical prisms will then deflect the beam by twice as much. The sign in (10) indicates a deflection towards the prism tip and consequently a plane wave hitting the structure in Fig. 1(*f*) will have all the crossover points at the same distance from the lens, which is its focal length, given by

$$f = h\tan(\gamma)/2\delta. \tag{11}$$

Note that this is equivalent to a single ($N = 1$) biconcave parabolic lens for a radius of curvature given by $R = h\tan(\gamma)$. Obviously the beam passing two prisms in Fig. 1(*e*) passes too much material at the greater distance from the tip of the second prism. An additional prism starts to deflect the beam for any increase in y by h. Consequently all large prisms could also be subdivided into chains of smaller prisms with identical height h. Here the passive material has to be removed according to (7) at the border between the jth row with j identical prisms and the row with $j + 1$ prisms. This limits the prism parameter h for a given wavelength λ to

$$h = \Delta m\lambda\tan(\gamma)/2\delta j. \tag{12}$$

Indeed h can be constant throughout the prism structure for $\Delta m = kj$, where $k > 0$ is an integer. Consequently in the present lens Δm increases linearly with distance y from the lens centre. This is equivalent to a lens composed of single elements per row, in which the segment height h is essentially constant, as shown in Fig. 2(*d*). In this case the segment width increases linearly with distance y from the optical axis. For the low-absorbing materials in the X-ray range, the sum $\sum_i N_i f_{1,i}$, which is the electron density of a material per unit volume, is essentially constant and thus from (2) one finds that δ/λ^2 is also almost constant. Consequently the same value for h is obtained for a fundamental wavelength λ and for all integer fractions λ/k of it. The possible focal lengths are then

$$f = \left(k\lambda/4\delta^2\right)\tan^2\gamma. \tag{13}$$

The arrangement of the small prisms can be compacted in this lens as shown in Fig. 1(*g*). With constant prism height h the final lens has simply become a linear transmission grating with very special blaze characteristics. Indeed, if the regular structure was perfect the intensity would be diffracted into only one order. With imperfections, the structure will instead produce diffraction orders with an angular separation of

$$\Delta\varphi = \lambda/h. \tag{14}$$

Actually, perfect prisms arranged in a row will only deviate a passing beam limiting the achievable focus size to the prism height h. A surprisingly simple correction will now make the highly symmetric prism structure ideally focusing. The derivative of the thickness $\mathrm{d}D'(y)/\mathrm{d}y$ for a parabolic CRL (Fig. 1*b*) is a linear function. For a perfect prism lens with identical f it is a step function with constant step width and with the same average slope. The difference (step function minus linear function) is a periodic function with constant negative linear slope. The implementation of this finding in the prism lens is straightforward, as can be seen in Fig. 1(*h*) and in Fig. 2. Both side surfaces of the single prism in the first row ($j = 1$) of the new lens (Fig. 2*c*) need to receive the corresponding curvature of the parabolic lens at a given y (Fig. 2*b*). In all other prism rows the same curvature needs to be repeated in only two of the many prism side walls. This correction is applied to the outermost prisms in any row in the lens array in Figs. 1(*h*) and 2(*c*). It is also very obvious in Fig. 3, which shows an example of our prototype lenses. The effective aperture of this lens for one-dimensional focusing is given by

$$\begin{aligned} A_{\mathrm{eff}} &= 2\sum_{j=1}^{J}\int_0^h \exp\left(-\frac{2j}{L\tan\gamma}y\right)\mathrm{d}y \\ &= L\tan\gamma\sum_{j=1}^{J}\frac{1}{j}\left[1-\exp\left(-\frac{2h}{L\tan\gamma}j\right)\right]. \end{aligned} \tag{15}$$

In the crossed lens configuration it will now allow an aperture of

$$A_{\mathrm{prism}} = Ph \tag{16}$$

in each direction

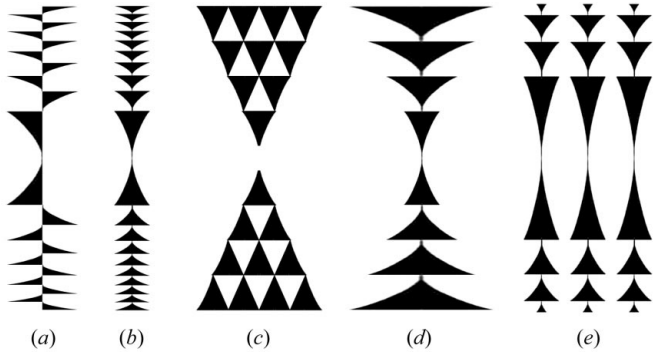

Figure 2
Comparison of kinoform transmission lenses of different design. All lenses or systems have identical focal length and are drawn to scale. Object (*a*) repeats the single lens from Fig. 1(*e*), (*b*) is equivalent and symmetric with respect to the vertical axis, (*c*) is the presented prism lens from Fig. 1(*h*), and (*d*) is the equivalent with single segments per row. (*e*) shows a stack of identical lenses of type (*b*).

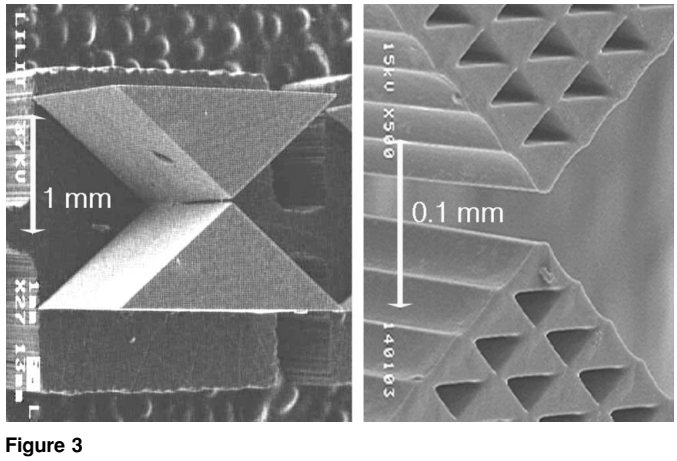

Figure 3
Scanning electron micrographs of one of the prototypes of the lens arrays produced by deep X-ray lithography. The left-hand part shows an overview, while the right-hand part shows details in the lens centre. This particular lens has a prism height of $h = 25.67$ µm, a prism angle of $\gamma = 35°$ and a geometrical aperture of $A = 1.8$ mm. For $k = 2$ this lens provides a focal length of $f = 2.14$ m. The array has all outermost prism walls curved identically and it was found to be etched uniformly over 0.6 mm into a 1 mm-thick SU-8 layer.

3. Lens parameter optimization

The lightest materials into which the structures can be transferred by deep X-ray lithography are the resists PMMA and SU-8. The latter is more radiation resistant and will thus be used (Singleton *et al.*, 2001; Cremers *et al.*, 2001). Beryllium cannot be considered for lithographic processes. The principle constituents in developed SU-8 with density 1.2 g cm^{-3} are polymer chains of composition $C_{22}O_4$ (Gelorme *et al.*, 1989). Heavier components S and SbF_6 are contained together with additional CO groups in the photoinitiator, which accounts for 2–6% of the resist mass. The hydrogen content is about one H atom for every C atom. The optimization and further lens comparisons will be made here for Cu K radiation ($\lambda = 0.154$ nm, $E = 8.05$ keV). SU-8 has, in this case, $\delta = 4.2 \times 10^{-6}$ and an attenuation length (for 4% photoinitiator content) of the order of $L = 1$ mm. With equation (7) this leads to $D(y) = m \times 36.67$ µm. With the prism angle $\gamma = 45^\circ$ and for $k = 1$ the lens will have, according to (12) and (13), $h = 18.34$ µm and $f = 2.183$ m. The absorption is such that the effective aperture according to (15) does not converge to a finite value. The effective apertures achievable with the geometric apertures of 1, 2 and 3 mm are 0.8, 1.32 and 1.7 mm, respectively. For demonstration purposes, lenses with geometrical apertures of 2.6 mm ($J = 71$) and 1.8 mm were optimized for one-dimensional focusing. For the earlier-discussed parameters and for $P = 25$ the possible aperture for two-dimensional focusing according to (16) is then only $A_{\rm prism} = 0.45$ mm. For the parameters of the lens in Fig. 3 with similar focal length $f = 2.14$ m it should be larger with $A_{\rm prism} = 0.63$ mm.

4. Lens production

The small prisms can be produced uniformly over these depths only by use of deep X-ray lithography (DXRL) in combination with synchrotron radiation exposure. This was carried out for the prototypes at the dedicated ELETTRA beamline (Pérennès *et al.*, 2001). This technique allows the reproduction of microstructures with very high aspect ratios P with optical-quality side-wall roughness (<30 nm) and with very low line-width non-uniformity over the structure height (Pantenburg & Mohr, 2001). DXRL's most common resists, PMMA and SU-8 (Singleton *et al.*, 2001; Cremers *et al.*, 2001), have similar optical properties in the X-ray range. However, they react differently to exposure to X-rays: while PMMA is selectively removed owing to chain scissions in the exposed regions (positive resist), the absorbed energy contributes to the crosslinking in SU-8. The latter resist is thus soluble only in the non-exposed areas (negative resist). The DXRL mask with positive and negative tone patterns suitable for the exposure of both resists was obtained in a two-step process. First an intermediate mask was produced by UV lithography and then it was replicated using soft X-rays (Schmidt *et al.*, 1999). After the final DXRL the structures etched into SU-8, which is also more resistant to the subsequent exposure to X-rays, showed better structural stability. No lens degradation owing to X-ray exposure was found during the subsequent experimental tests over the course of nine months.

5. Experimental results and discussion

The lens arrays were tested behind double-crystal monochromators [Si(111)] at the SYRMEP bending-magnet beamline at ELETTRA (SYRMEP, 2003) and at the undulator beamline ID22 at ESRF (ID22, 2003) in vertically focusing set-ups. At SYRMEP the photon energy was set to 8.35 keV, slightly above the projected value of 8 keV, which was then applied at ID22. At ELETTRA a CCD camera was mounted in the image plane, and at ESRF a diode was mounted slightly downstream of it. The intensity was registered with vertical slit scans in two different configurations. At ELETTRA the scan of a slit with an opening of 0.1 mm through the beam in front of the lens permitted the characterization of its focusing properties depending on the position at the lens. At the ESRF the scan of a slit with a smaller opening of 7 µm through the beam in the image plane permitted the determination of the image size.

Even though the resist had a thickness of 1 mm, it was found from X-ray radiographs that the etching had stopped abruptly at a depth of about 0.4 mm for prisms with $h = 18.34$ µm and at a depth of about 0.6 mm for $h = 25.67$ µm ($f = 2.14$ m for $k = 2$). Over these depths, which are consistent with the expectations, the prisms showed uniform focusing behaviour. As expected, the prism array transmission $t(y)$ varied symmetrically with respect to the lens centre ($y = 0$). In the unetched part, *i.e.* in a single large prism, the beam was deflected by the constant angle from (10). Here the measured transmission varied according to $T = \exp[-M(y)/L]$ with $L = 1.175$ mm. The latter number is slightly larger than expected and points to a photoinitiator content of below 4% in the SU-8 grade utilized here. The X-ray radiograph of the etched region revealed a transmission consistent with the observed material distribution as shown in Fig. 3. Indeed, the single-prism rows contain 22% more material than projected as the holes are found to have reduced dimension. The solid line in Fig. 4 (top) presents the best-fit curve to the latter transmission data in the lens aperture of 2.6 mm. In a perfect lens array the refraction efficiency $\varepsilon(y)$, *i.e.* the normalized flux refracted at a given lens position y into the fixed focus, should be identical to the transmission function $t(y)$. The experimental refraction efficiency $\varepsilon(y)$ (circles in Fig. 4) was obtained from the respective slit scan by integrating the intensity registered at the fixed image position over a spot size of 56 µm. Within this spot size, which would cover the −1st-, 0th- and 1st-order diffraction peaks, no smaller features could be resolved at SYRMEP in a knife-edge scan with 4 µm step size. From Fig. 4 one sees that the refraction efficiency is obviously smaller than expected. Nevertheless, even outermost rows with as many as 64 prisms still refract part of the transmitted intensity into the image. Compared with the ideal transmission curve

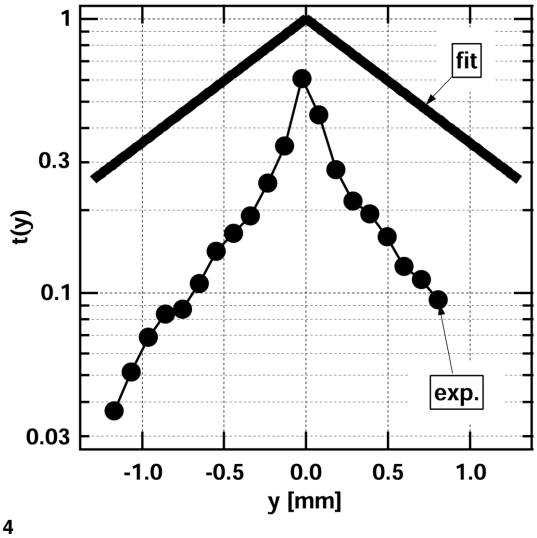

Figure 4
Dependence of the array transmission (solid curve labelled 'fit') and its refraction efficiency (circles) on position in the lens. The solid curve is the best fit to the lens transmission function $t(y)$ as obtained from radiography images recorded 15 cm behind the lens. The circles represent the normalized flux measured in a slit of width 56 µm at the focus position depending on the illuminated position at the lens.

(solid line), the refraction efficiency falls off approximately with a $j^{-1/2}$ dependence, which is consistent with randomly distributed surface irregularities at the prism side walls. The observed gain of 10 and the full-width-at-half-maximum focus width of 50 μm lead to an experimental effective aperture of $A_{\rm eff,exp} = 0.5$ mm. Theoretically, a value of $A_{\rm eff} = 1.65$ mm was expected from (15) for $J = 71$ and $L = 1.175$ mm. Cylindrical CRLs with identical focal length produced with $d = 0$ in SU-8 and in beryllium would have ideally provided $A_{\rm eff}$(SU-8) = 0.082 mm and $A_{\rm eff}$(Be, $L = 6$ mm, $d = 4.9 \times 10^{-6}$) = 0.63 mm, respectively. Reported lenses in the latter material have either $R_1 = 1.9$ mm and $d_1 = 0.04$ mm (Beguiristain *et al.*, 2002) or $R_2 = 0.20$ mm and $d_2 = 0.17$ mm (Schroer *et al.*, 2002). For a focal length of the order of $f = 2.15$ m, it needs $N_1 = 85$ lenses of the first kind and $N_2 = 9$ of the latter. Consequently, with $N_1 d_1 = 3.4$ mm and $N_2 d_2 = 1.53$ mm, their effective apertures are reduced to $A_{\rm eff,1} = 0.36$ mm and $A_{\rm eff,2} = 0.49$ mm. From this comparison it is clear that only refractive lenses in beryllium have the potential to exceed the effective apertures of the presented new lenses, while all other materials with more absorption will perform worse.

At ID22 of the ESRF the spot size in the image plane of the lens was measured by limiting the incident beam horizontally to 0.4 mm, *i.e.* the uniform prism depth. In this case we limited the vertical beam acceptance to 0.5 mm, corresponding to an effective aperture of 0.4 mm, for several reasons. Firstly, a 2.6 mm beam size was not available. Secondly, the diffraction patterns from the two lens halves did not overlap, which was to be expected as the gap between the two lens halves was too large. In addition, the realized lenses with excess material provided more phase shift than projected, which results in phase discontinuities behind the lens. With the symmetry of the object, the diffraction patterns from the two lens halves will then only coincide for a particular gap between them. The latter would be different from the projected gap. The phase discontinuities will also take away intensity from the zeroth-order peak. Actually, the real lens structure would have provided minimum phase discontinuities according to (7) for a photon energy of 8.5 keV, which, however, was not used for the experiment. Finally, only one half of the lens was illuminated with a vertical beam size of 0.5 mm. A slit with an opening of 7 μm was scanned vertically through the image at various image distances. The intensity measured behind the aperture at the optimum image distance of 2.309 m is shown in Fig. 5. The expected diffraction pattern with a periodicity of 19.4 μm is clearly resolved. The pattern is not symmetric with respect to this zeroth-order peak owing to the asymmetric transmission function of the illuminated lens half. From the plateau-like shape of the peaks and the valleys of the measured intensity curve, one immediately deduces a diffraction-peak width of less than 7 μm. The derivative of the curve provides a more quantitative result. The slit scan can then be considered a double knife-edge scan with two opposing blades. The derivative of the intensity curve should then always result in two perfectly anti-symmetric peaks around any intensity peak. The expected peak symmetry is observed, and the mean value derived for the full width at half-maximum (FWHM) of the three central diffraction orders is 2.8 μm. This is only about 50% larger than the expected image size of 1.73 μm, which should have been obtained with a lens of focal length $f = 2.183$ m positioned 40 m from a source with a vertical extent of 30 μm (ID22, 2003). Considering the obvious imperfection of the realized lens, this is a surprisingly good result. The photon flux density gain in the zeroth-order peak is 23, which then results in an observed effective aperture of about 0.065 mm. Note that both values would have been twice as high if the diffraction patterns from both lens halves had overlapped. Even though rather small, the effective aperture observed here is larger than the reported values for the normal kinoform lenses (Aristov *et al.*, 2000). These latter lenses provided a similar or about twofold-smaller focus size than reported here; however, they cannot yet provide submicrometre focii. The present observed effective aperture would double if one sums the intensity over the central three diffraction orders. Then the relative performance compared with the theoretical value of 0.4 mm is consistent with the earlier-described observations at SYRMEP. If one integrates over all observed orders, the related effective aperture is almost 0.3 mm. Consequently the concentration of relatively more intensity into the zeroth diffraction order expected from a more regular prism structure could increase the effective aperture significantly.

In order to remove the unwanted diffraction orders of the present lens for microscopy experiments, one can simply position an aperture of size 10 μm at about 10 mm upstream of the sample without interfering with the sample and the principal diffraction peak. Smaller images of submicrometre dimensions are feasible with shorter focal lengths f by reducing the only free parameter γ in (13). Indeed, lenses with $\gamma = 35^\circ$ and $h = 12.8$ μm have already been successfully produced and have undergone some preliminary tests. However, these lenses still have $f = 1.07$ m. Values of $f = 0.54$ m and thus possible image sizes of $s' = 0.4$ μm would be possible using the slightly smaller values of $\gamma = 26.6^\circ$ and $h = 9.2$ μm. The latter lens has theoretical effective apertures of 0.7 mm and 1.0 mm for geometric apertures of 1.0 mm and 1.8 mm. Production of these lenses is underway, and the quality control of these easily replicable lenses with rather large prisms is facilitated by the fact that they can be made in a laboratory microscope using visible light.

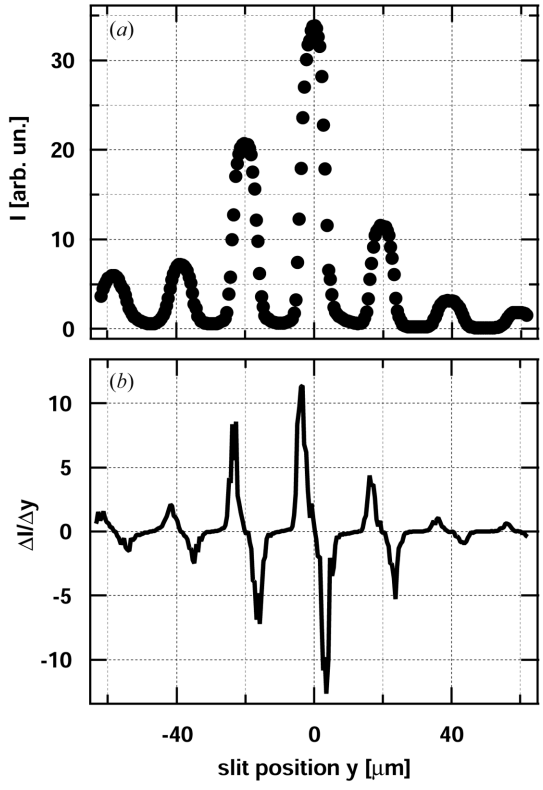

Figure 5
Imaging properties of the lens array. (*a*) Intensity distribution measured in the vertical direction at the optimum image distance with a slit of 7 μm aperture. The highest peak is the zeroth-order diffraction peak. (*b*) Derivative of the intensity distribution of (*a*).

An interesting feature of the lens has to be mentioned for the condition when the central three diffraction peaks cannot be resolved, as at the SYRMEP beamline at ELETTRA. In this case, with $f = 2.18$ m the intensity is refracted into spot diameters of about 50 µm. In tests, several crossed lens pairs for two-dimensional focusing provided intensity gains of at least 25 for this image size. The measured effective collection area was then about 0.06 mm^2 for a theoretical effective area of 0.4 mm × 0.4 mm = 0.16 mm^2. This performance is readily obtainable over the rather large variation of 100 mm in the image distance and without almost any lens alignment in tilt angle (0.2°). Consequently, such a lens pair, consisting of two lenses each measuring only about 3 mm × 3 mm × 3 mm, could be added rapidly into X-ray diffraction and small-angle X-ray scattering beamlines when a small sample is to be investigated.

6. Conclusion

It has been shown that, by removing passive material in increasing quantities from a transmission lens, a highly regular structure can be obtained which will focus X-rays similarly to kinoform transmission lenses but with significantly increased feature sizes. This latter property permits the production of lenses with rather large aperture in the focusing direction in the millimetre range and with depths in the perpendicular direction of 0.4–0.6 mm. The lenses present experimentally the predicted refraction and diffraction behaviour. The smallest image size measured, 2.8 µm, is only about 50% larger than expected. On the other hand, the effective aperture for focusing this image size falls behind expectation. This is assigned to the apparent imperfection of the lens, which spreads the diffracted intensity over several diffraction orders.

We gratefully acknowledge L. Singleton and A. Tunayar from the Institut für Mikrotechnik IMM (Mainz, Germany) for the excellent work on the lithography masks, which was supported by the European Union within the EMERGE proposal of IMM (contract No. HPRI-CT-1999-00023). We gratefully acknowledge one of the referees for his careful study of our report and his suggestion to use the concept of effective aperture for the comparison of different X-ray transmission lenses.

References

Aristov, V., Grigoriev, M., Kuznetsov, S., Shabelnikov, L., Yunkin, V., Weitkamp, T., Rau, C., Snigireva, I., Snigirev, A., Hoffmann, M. & Voges, E. (2000). *Appl. Phys. Lett.* **77**, 4058–4060.

Beguiristain, H. R., Cremer, J. T., Pietrup, M. A., Gary, C. K. & Pantell, R. H. (2002). *Opt. Lett.* **27**, 778–780.

Bilderback, D. H., Hoffman, S. A. & Thiel, D. J. (1994). *Science*, **263**, 201–203.

Cederström, B., Cahn, R. N., Danielsson, M., Lundqvist, M. & Nygren, D. R. (2000). *Nature (London)*, **404**, 951.

Chantler, C. T., Olsen, K., Dragoset, R. A., Kishore, A. R., Kotochigova, S. A. & Zucker, D. S. (2003). *X-ray form factor, attenuation and scattering tables*, http://physics.nist.gov/ffast. [Originally published as Chantler, C. T. (2000). *J. Phys. Chem. Ref. Data*, **29**, 597–1048; and Chantler, C. T. (1995). *J. Phys. Chem. Ref. Data* **24**, 71–643.]

Cremers, C., Bouramrane, F., Singleton, L. & Schenk, R. (2001). *Microsyst. Technol.* **7**, 11–16.

Di Fabrizio, E., Romanato, F., Gentili, M., Cabrini, S., Kaulich, B., Susini, J. & Barrett, R. (1999). *Nature (London)*, **401**, 895–898.

Gelorme, J. D., Cox, R. J. & Gutierrez, S. A. R. (1989). US Patent 4 882 245.

Henke, B. L., Gullickson, E. M. & Davis, J. C. (1993). *Atom. Data Nucl. Data Tables*, **54**, 181–342. (http://www-cxro.lbl.gov/optical_constants/.)

Hignette, O. *et al.* (2004). To be published.

ID22 (2003). *ID22 micro-fluorescence, imaging and diffraction*, http://www.esrf.fr/UsersAndScience/Experiments/Imaging/ID22/.

Jark, W., Cedola, A., Di Fonzo, S., Fiordelisi, M., Lagomarsino, S., Kovalenko, N. V. & Chernov, V. A. (2001). *Appl. Phys. Lett.* **78**, 1192–1194.

Kirkpatrick, P. & Baez, A. (1948). *J. Opt. Soc. Am.* **38**, 766–774.

Lengeler, B., Schroer, C. G., Richwin, M., Tuemmler, J., Drakopoulos, M., Snigirev, A. & Snigireva, I. (1999). *Appl. Phys. Lett.* **74**, 3924–3926.

Lengeler, B., Schroer, C. G., Tuemmler, J., Benner, B., Richwin, M., Snigirev, A., Snigireva, I. & Drakopoulos, M. (1999). *J. Synchrotron Rad.* **6**, 1153–1167.

Lesem, L. B., Hirsch, P. M. & Jordan, J. A. Jr (1969). *IBM J. Res. Dev.* **13**, 150–155.

Pantenburg, F. J. & Mohr, J. (2001). *Nucl. Instrum. Methods*, A**467**/**468**, 1269–1273.

Pérennès, F., De Bona, F. & Pantenburg, F. J. (2001). *Nucl. Instrum. Methods*, A**467**/**468**, 1274–1278.

Pfeiffer, F., David, C., Burghammer, M., Riekel, C. & Salditt, T. (2002). *Science*, **297**, 230–234.

Schmidt, A., Adam, D., Belic, N., Burkhard, F., Hartmann, H., Hoke, F., Himmelsbach, G., Lüttge, R., Schacke, H. & Wolf, H. (1999). *16th European Conference EMC on Mask Technology for Integrated Circuits and Micro-Components '99*, pp. 151–157 Berlin: VDE-Verlag.

Schroer, C. G., Kuhlmann, M., Hunger, U. T., Günzler, T. F., Kurapova, O., Feste, S., Frehse, F., Lengeler, B., Drakopoulos, M., Somogyi, A., Simionovici, A. S., Snigirev, A., Snigireva, I. & Schug, C. (2003). *Appl. Phys. Lett.* **82**, 1485–1487.

Schroer, C. G., Kuhlmann, M., Lengeler, B., Günzler, T. F., Kurapova, O., Benner, B., Rau, C., Simionovici, A. S., Snigirev, A. & Snigireva, I. (2002). *Proc. SPIE*, **4783**, 10–18.

Singleton, L., Bogdanov, A. L., Peredkov, S., Wilhelmi, O., Schneider, A., Cremers, C., Megtert, S. & Schmidt, A. (2001). *Proc. SPIE*, **4343**, 182–192.

Snigirev, A., Kohn, V., Snigireva, I. & Lengeler, B. (1996). *Nature (London)*, **384**, 49–51.

Snigireva, I., Snigirev, A., Rau, C., Weitkamp, T., Aristov, V., Grigoriev, M., Kuznetsov, S., Shabelnikov, L., Yunkin, V., Hoffmann M. & Voges, E. (2001). *Nucl. Instrum. Methods*, A**467**, 982–985.

Suehiro, S., Miyaji, H. & Hayashi, H. (1991). *Nature (London)*, **352**, 385–386.

SYRMEP (2003). *BL 6.1 R, SYnchrotron Radiation for MEdical Physics (SYRMEP)*, http://www.elettra.trieste.it/experiments/beamlines/syrmep/index.html.

Tomie, T. (1994). Japanese Patent 6 045 288.

Yang, B. X. (1993). *Nucl. Instrum. Methods*, A**328**, 578–587.

Yun, W., Lai, B., Cai, Z., Maser, J., Legnini, D., Gluskin, E., Chen, Z., Krasnoperova, A. A., Vladimirsky, Y., Cerrina, F., Di Fabrizio, E. & Gentili, M. (1999). *Rev. Sci. Instrum.* **70**, 3537–3541.